Recursive Imaging with Multiply-Scattered Waves Using Partial Image Regularization: A North Sea Case Study

Alison E. Malcolm* Maarten V. de Hoop† and Bjørn Ursin⋆
* Department of Earth, Atmospheric and Planetary Sciences, Massachusetts Institute of Technology †
Department of Mathematics and Department of Earth Sciences, Purdue University
⋆ Norwegian University of Science and Technology Department of Petroleum Engineering and Applied Geophysics S. P. Andersens vei 15A, NO-7491, Trondheim, Norway

Abstract

As more resources are directed toward reverse-time migration an accurate velocity model, including strong reflectors, is necessary to form a clear image of the subsurface. This is of particular importance in the vicinity of salt, where singly-scattered waves are often not ideal for imaging the salt flanks. This has led to interest in processing doubly-scattered waves (also called duplex or prismatic waves) for imaging salt flanks and thus improving the location of salt boundaries in a velocity model. We present a case study in which we use doubly-scattered waves in a two-pass one-way method to image salt flanks in a North Sea data set. By working in the one-way framework we are able to separately construct images with singly, doubly, and triply scattered waves. We illustrate a multi-step imaging process that includes multiply-scattered waves by using an imaged reflector to fix one (or more) of the scattering points, allowing for multiply-scattered energy from several reflectors, potentially with poor continuity, to be included without picking each reflector individually. With this method we are able to image the flank of a North Sea salt body.

Introduction

In two related papers, Farmer et al. (2006) and Jones et al. (2007), show how so-called prismatic reflections (doubly-scattered waves) can be included in a reverse-time migration procedure, by including a reflector in the velocity model, to improve the location of salt flanks in a North Sea data set. We use the same data set to demonstrate a recursive, data driven, one-way approach we introduced in Malcolm et al. (2009). There are several advantages to using a such an approach for this imaging problem. The first is that in the recursive approach a standard image (i.e. an image made with a standard migration algorithm assuming that all of the recorded signal comes from singly-scattered waves) is used as an estimate of the location and amplitude of the multiple-generating interface, removing the need to pick a reflector and include it in the background velocity model; for this data set this moves the imaged salt flank. (We will use the word 'multiple' here to refer to any wave that has scattered more than once, thus doubly-scattered, prismatic, or duplex waves are considered multiples.) In addition, by imaging in a one-way approach we have control of the various wave constituents and their direction of propagation. This allows separate images to be produced from singly, doubly and triply-scattered waves; the total image is simply the sum of these contributions. It is then possible to interpret these images separately, and to highlight and remove any artifacts from each image. The use of one-way methods, although limiting somewhat in terms of high-angle accuracy, reduces the computational cost of the procedure.

Doubly-scattered waves, referred to as either duplex waves or prismatic reflections in the literature, have been considered as a source of additional information for some time. In Bell (1991), they are used to explicitly locate a vertical reflector by reducing the traveltime of a doubly-scattered wave to that of a primary. The effect of doubly-scattered waves on dip move-out algorithms is discussed by Hawkins (1994). Bernitsas et al. (1997) demonstrates the artifacts expected in subsalt imaging from prismatic reflections. In a more modern imaging context, Marmalyevskyy et al. (2005) uses a ray-theoretic approach and an explicitly picked near-horizontal reflector to image a near-vertical reflector with doubly-scattered waves; this is adapted and applied to a real data set by Link et al. (2007). The work of Broto and Lailly (2001); Cavalca and Lailly (2005, 2007) also uses ray theory and doubly-scattered waves, but in the context of developing an inversion algorithm that allows for regions in which particular events are not recorded or do not exist. This is particularly important for doubly-scattered waves as they are rarely recorded throughout the survey extent. Most recently, Marmalyevskyy et al. (2008); Kostyukevych et al. (2009) compute transmission coefficients for doubly-scattered waves to allow their migration in a Kirchhoff method for a VSP geometry in fractured media.

Our method for imaging with multiply-scattered waves has similarities to the two-pass one-way methods proposed first by Hale et al. (1991) for imaging turning waves, in which the wavefield is first propagated down into the subsurface and stored at depth and then propagated back to the surface in a second pass. More recent discussions of these methods can be found in Xu and Jin (2006) and Zhang et al. (2006). The difference between turning wave imaging and doubly-scattered wave imaging is in the inclusion of a reflection from the lower boundary. This was done using the multiple-forward, single back-scatter method in Jin et al. (2006); Xu and Jin (2007). By contrast, we use a standard image to approximate the strength and location of the multiple-generating reflector, rather than explicitly including this reflector in the velocity model. Specifically, within a shot-record migration algorithm, we first propagate the wavefield down into the subsurface, then multiply by the reflectivity estimated from the standard image; the resulting composite wavefield is then propagated upwards and an image is formed from the interference of the source and data wavefields. The use of an image to approximate the location and strength of the multiple-generating reflector also sets our method apart from the reverse time methods mentioned above (Farmer et al., 2006; Jones et al., 2007), in which the reflector is included in the velocity model. Our method assumes that multiples do not generate artifacts in this singly-scattered image, or that they have been removed.

There is no fundamental difference between imaging with doubly and triply-scattered waves (multiples). Thus far, however, most imaging with multiply-scattered waves has focused on surface-related multiples as these are the simplest to understand and the closest, in many ways, to singly-scattered waves because the multiple-generating reflector is well known (sea surface). Beginning with the work of Reiter et al. (1991) who proposed a method for imaging with water-column multiples in a Kirchhoff scheme and continuing through the recent work of Berkhout and Verschuur (2003, 2004, 2006) in which surface-related multiples are converted into primaries, surface-related multiples have been shown to provide added information in imaging. Brown and Guitton (2005) discusses a unified framework to image with both primaries and surface-related multiples, focussing on removing cross-talk between the different

images. There are also several discussions for particular acquisitions, such as VSP (Jiang, 2006) and OBC (Muijs et al., 2007) as well as more in depth inversion procedures such as that suggested by Métivier et al. (2009). For the more complicated situation of internal multiples, most studies exploiting these events rely on interferometry to record at depth and subsequently convert internal multiples into primaries (Schuster et al., 2004; Jiang et al., 2005, 2007; Vasconcelos et al., 2007). These methods are somewhat similar to the Berkhout and Verschuur (2006) methods in that they remove one leg of the propagation via cross-correlation. Mittet (2002, 2006) discusses the inclusion of multiples in reverse-time migration with a specific focus on data requirements for multiples to image correctly, without causing artifacts in the image. Youn and Zhou (2001) describe a method, based on finite differences, that allows for the simultaneous imaging of primaries, internal and surface-related multiples that requires detailed velocity information and requires additional computational resources compared to other methods.

As is to be expected, when imaging with the relatively low amplitude multiply-scattered waves data sampling becomes more important than for the singly-scattered case. There are many different ways of interpolating and filling in data; a relatively recent review of methods can be found in e.g. Stolt (2002). Here, we chose to use a wave packet based method that both fills in missing data and denoises concurrently, through sparsity promoting optimization. This method of regularizing data goes back to Daubechies and Teschke (2005), in which iterative thresholding was applied to images in order to simultaneously deblur and denoise them. This method was developed further for the seismic case by Hennenfent and Herrmann (2006), in which they discuss the curvelet transform, introduced in Candès et al. (2006), with particular emphasis on nonuniformly sampled data. More details on the algorithm used here can be found in Andersson et al. (2010).

This paper has three main sections, the first summarizes the imaging with multiples method as well as the regularization method. The second uses synthetic data to illustrate sampling issues when imaging with multiply-scattered waves and the third discusses the application of the methods to a data set from the North Sea.

Summary of Methods

The procedure for imaging with multiply-scattered waves employed here is discussed in detail in Malcolm et al. (2009), here we give a summary of the most important ideas, without discussing the underlying theory. The method builds on previous work in Malcolm and de Hoop (2005) which combines two series approaches, the Generalized Bremmer series (de Hoop, 1996) and the Born series discussed by Weglein et al. (2003).

The basic structure of our technique for imaging with multiply-scattered waves is straightforward. The procedure is broken into the following steps, illustrated in Figure 1,

1. Form a standard image, defined as a migrated image using any standard imaging technique, that assumes singly-scattered waves.

2. Propagate the surface data down into the subsurface (with a one-way method), as in a standard shot-record migration. At each depth, multiply the wavefield by the image,

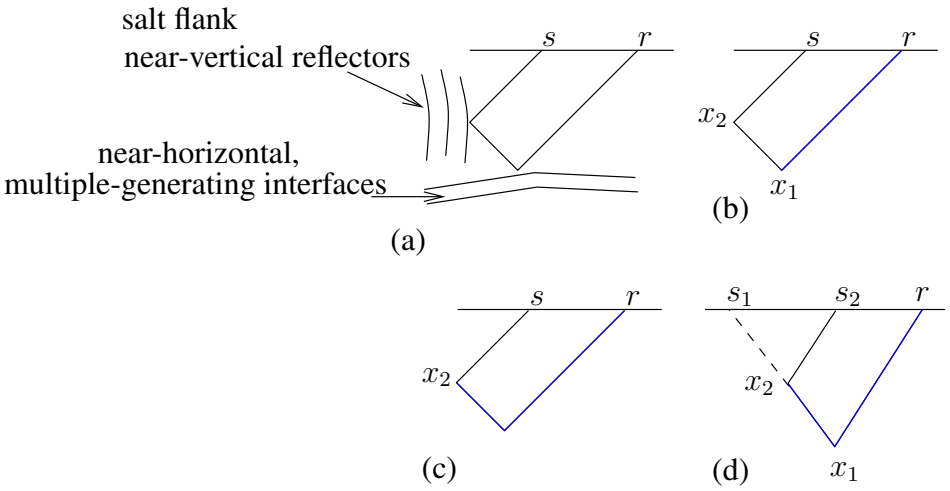

Figure 1: (a) Ray path for a doubly-scattered wave, like those used here to image the salt flank. (b) In black is an illustration of the part of the raypath that will remain once the data for a single shot are propagated into the subsurface to the first scattering point at x_1 (i.e. we remove the propagation along the blue part of the path). At x_1 the downward propagated wavefield is multiplied by an estimate of the reflectivity at x_1, here approximated by the amplitude of the image at x_1. (c) The resulting composite wavefield is then propagated upward to x_2 (again illustrated with raypaths in blue) where an image is formed by crosscorrelating this up-going field (blue) with the downward propagated source wavefield (black). (d) With this imaging condition, primaries with raypaths along the solid blue path from r to x_1 to x_2 continuing along the dashed path from x_2 to the surface will interfere constructively along the entire path, creating artifacts. Here, we attenuate these artifacts by using an f-k filter to separate these events before applying the imaging condition (primaries (dashed) propagate to the left after x_2 in this cartoon while doubly-scattered waves propagate to the right (solid black) after x_2; they share the blue part of the path).

formed in 1, and store the resulting composite wavefield at each depth (Figure 1(b)). This models the reflection of the wavefield from the multiple-generating interface, approximated by the image made in 1.

3. Propagate the composite wavefield up to the surface (Figure 1(c)), forming an image at each depth by applying a crosscorrelation imaging condition to the two composite wavefields for internal multiples, and to one composite wavefield (traveling along the blue ray in Figure 1c) and the standard downward continued wavefield (traveling along the solid black path in Figure 1c) for doubly-scattered waves.

As in reverse-time migration, including multiples requires the specification of a layer (or multiple layers) that generate the multiples (see the discussion in Jones et al. (2007)). In other words, referring to Figure 1, to make an image at x_2 an estimate of the reflectivity at x_1 is required. This information must be included directly in the velocity model for reverse-time migration, and for the methods of Jin et al. (2006); Xu and Jin (2007). In our method this information is included separately, and is obtained directly from a standard image, as this is the best estimate we expect to have of the reflectivity itself. This means that only the regions of the image (and, if the image is accurate, of the Earth) that have significant reflectivity contribute to the generation of multiply-scattered waves, and that it is not necessary to specify explicitly all layers that may generate multiples. Of course, it is still possible to exclude multiples from specific layers by simply muting the input image to not include those layers. It is thus not necessary that there be a single coherent reflector, forming the x_1 imaging points in Figure 1, for all doubly-scattered waves, although there must be something that physically reflects the energy toward the salt flank (in other words doubly-scattered waves must be generated by the Earth adn recorded at the surface).

Similar to methods discussed by Brown and Guitton (2005), imaging with multiply-scattered waves requires the separation of these multiples from primaries. Although a method such as that suggested by Brown and Guitton would likely result in a cleaner image with fewer artifacts, we have found that much simpler procedures are adequate, in particular for doubly-scattered waves. For these waves, we observe that most of the artifacts come from the interference of doubly-scattered waves with primaries that share part of the path of the doubly-scattered waves as illustrated (blue rays) in Figure 1(d). These waves can be removed in a straightforward manner by applying an f-k filter before applying the imaging condition, to separate left- and right-going waves, thus allowing the imaging condition to be applied to wavefields traveling in opposite horizontal directions, thus removing artifacts from primaries. In the example studied here, we find the best results using a filter that tapers to zero over several wavelengths, removing waves up to vertical propagation from both the source and receiver-side wavefields; we found that using a smooth filter was more important than the specific location of the cut-off wavenumber.

ℓ_1 regularization

The basic idea of this regularization method is to first take the curvelet transform of the data, (discussed in Candès et al. (2006)), which results in a decomposition of the data as a func-

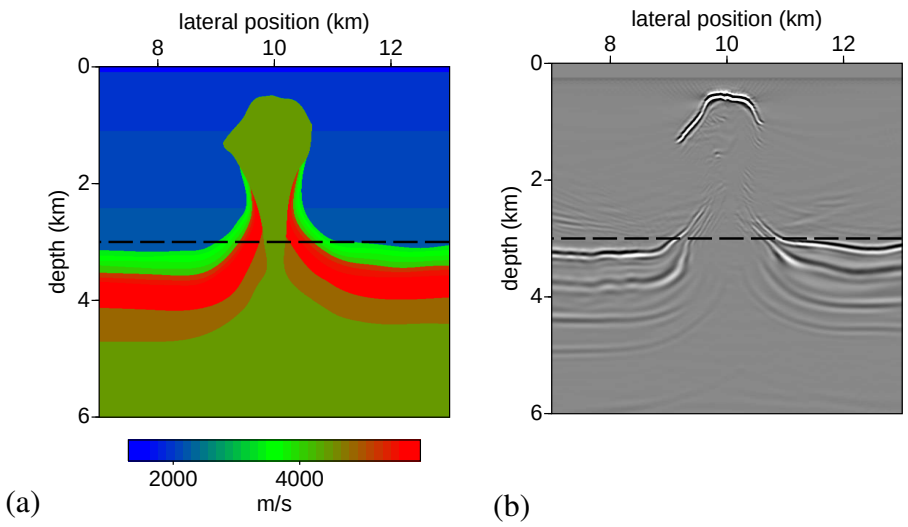

Figure 2: (a) Velocity model used to generate the synthetic data set. (b) Standard migration image made using data generated in the velocity model in (a), assuming single scattering.

tion of scale and orientation. Scale gives a measure of the coherency of the wavefield in a particular (spatial) frequency band; coherent structures are at large scales whereas incoherent structures exist over a range of smaller scales. Orientation indicates the direction of the wave packet. We then apply a thresholding and regularization/interpolation in the curvelet domain, similar to that introduced by Daubechies and Teschke (2005) and extended by Hennenfent and Herrmann (2006). It is in this regularization procedure that an ℓ_1-norm (the sum of absolute values) is used; this norm is used because it promotes sparsity (few non-zero curvelet coefficients) which keeps the fewest coefficients necessary to explain the data. In the thresholding procedure, discussed further in Andersson et al. (2010), small scales are removed, to lower the ambient noise level of the signal by removing incoherent events. This is conceptually similar to a low-pass filter although in this case the filter is applied in a domain specifically tailored to wave problems (meaning that seismic data are sparse in the curvelet domain), allowing for the ℓ_1 regularization that promotes sparsity. To regularize the data, the output of the inverse curvelet transform is computed at a denser grid than the input data. The advantage of this procedure over a bandpass filter and Fourier domain sinc interpolation is in the sparsity-promoting ℓ_1 regularization that is applied in the curvelet domain where (noise-free) seismic data are expected to be sparse.

Effect of Sampling

To illustrate the importance of sampling in the lateral direction, we begin with a synthetic data set with several near-vertical layers (i.e. structures with very large dip), designed to mimic the structures seen in the real data set discussed in the following section. The velocity model

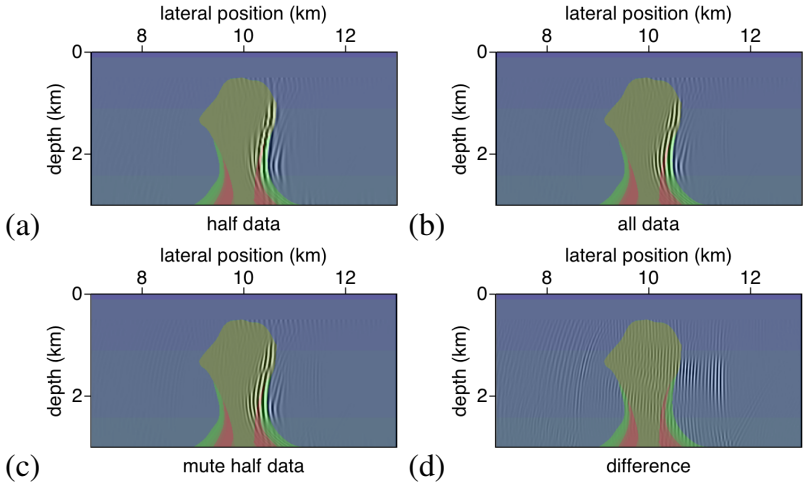

Figure 3: The effect of grid size on the final image. (a) Using a receiver spacing of 25 m we get a good image of the vertical salt-flank. (b) Using a receiver spacing of 12.5 m gives the image a higher resolution, although the location and shape of the reflector do not change much. (c) Using the same grid as in (b) for the propagation, but with every second receiver muted (so an effective receiver spacing of 25 m with an actual receiver spacing of 12.5 m) gives nearly the same image as in (b) indicating that the additional data is not required but forming the image on a finer grid improves the image. (d) Is the difference between (b) and (c), shown with amplitudes clipped at 1/20 of the value in (c). All of these figures were made using the image shown in Figure 2 muted outside the interval 2.5-3.4 km as the input singly-scattered image and a smoothed version of the velocity model shown in Figure 2 as the migration velocity model.

for this data set is shown in Figure 2, along with a standard image made with a shot-record migration using a simple phase-shift propagator, performing the phase-shift separately for each velocity occuring in a horizontal slice. This is similar to the PSPI propagator (Gazdag and Sguazzero, 1984) as well as to the propagators suggested in Ferguson and Margrave (2002). Although the cost is somewhat prohibitive when using a lot of velocities, it is easy to implement and we find this propagator to be sufficiently accurate for this data set. Either this propagator or a simple split-step propagator are used throughout this paper. Any other one-way propagator could be used in place of either of these methods; our goal is not to investigate propagators and so we chose the simplest propagator to implement that gave reasonable results for the models used. In principal, nothing will change by changing the propagator provided it estimates the wavefield sufficiently accurately.

Resolving the different vertical layers in this model requires that the image be made on a relatively dense horizontal grid. Because the goal is to image near (and beyond) vertical layers good lateral resolution is required to image and separate the different layers. This does not mean that more data is required than is used to make a standard image, only that the image may need to be formed on a denser grid than that which the data are collected on. This is illustrated in Figure 3. In this figure two different receiver sampling intervals are used to form the doubly-scattered image, both of which are sufficient to see the flank of the salt, but the denser of which (in (b)) has better resolution. We also illustrate, by muting the recordings from every other receiver for all shots in the data set used to make the more densely sampled image, that more data is not required as the images in (b) and (c) are nearly equivalent ((d) shows the difference between these two images, clipped at 1/20 of the image in (c)). The image shown in Figure 2(b), muted outside of depth 2.5 to 3.4 km, is used for the input singly-scattered image. All three images have significant ringing. This is caused by a combination of (i) the truncation of the f-k filter used to separate doubly-scattered waves from primaries, (ii) multiply reflected waves between the different vertical layers and (iii) the convolution of an extra wavelet from the use of an image as an estimate of reflectivity. It is expected that the second cause is dominant because, as will be illustrated with a simpler synthetic in the discussion, simpler models (in which cause (i) and (iii) are unchanged) have significantly less ringing than the images made in this model or the real data set.

Application to North Sea Data Set

In this section we explore the possibility of using doubly-scattered waves to improve the velocity model near a salt structure that is not well imaged. The data are from a North Sea field; this data set is discussed in more detail in Farmer et al. (2006); Jones et al. (2007), where a similar set of procedures are applied in a reverse-time migration framework. What this study adds is, first the removal of the requirement that the salt itself be included in the velocity model, and second the requirement that hard boundaries be included in the velocity model. The first requirement is removed by using only waves that travel outside the salt to image its boundaries. This is similar to the result in Jones et al. (2007) that used reverse time migration to image the salt flanks with duplex waves. The second requirement is removed by separating the smooth background velocity model, through which the waves are propagated, from the sharp

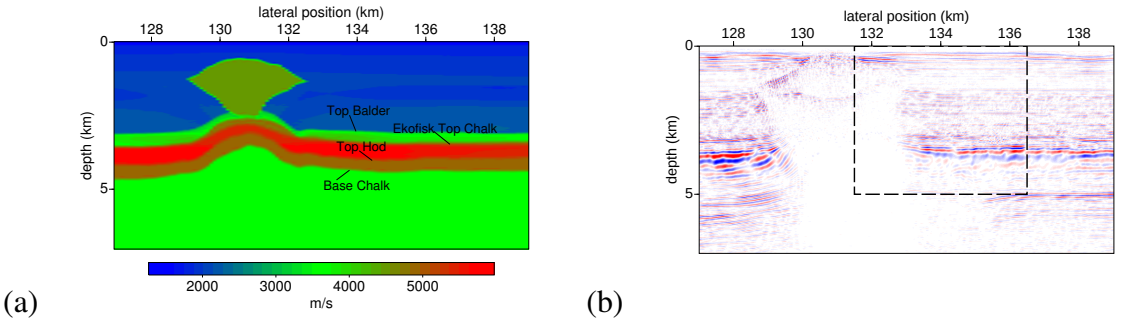

Figure 4: (a) Original velocity model for the real data set. Three different models are used in this case study, the full model, depicted here, the sediment model, which does not include the salt itself and the 1D model which is the velocity as a function of depth at the first lateral position (approximately 127 km). (b) Image made with the original data set, including offsets up to 2 km, and using the sediment model.

interfaces from which the waves reflect. By using both an image (for the reflectivity) and a velocity model (through which to propagate waves), we are able to reduce the requirements on the level of detail present in the migration velocity model. The velocity model, estimated through one-way tomography, as discussed in Jones et al. (2007), is shown in Figure 4(a). The images formed here use either this model with the salt removed (sediment velocity model) or a 1D model consisting of the velocity as a function of depth at the first lateral position (approximately 127 km). The 1D model was used to test the impact of lateral variations in the model on the resulting images. Figure 4(b) shows an image made with all 315 recorded shots on a 2D line extracted from the 3D volume, for each shot 120 offsets are recorded with a minimum offset of 160 m and 25 m spacing; the shot spacing is 50 m. To avoid artifacts caused by waves traveling through the salt, we limit the offsets included in the imaging to 2 km; the image was made with a split-step propagator.

From the migrated image in Figure 4 we see that there is likely a salt dome between approximately 129 and 133 km that is precluding the formation of an image in that region. To improve our ability to image this structure, we first form an image with doubly-scattered waves using data recorded to the right of the salt, using 50 shots from 135 to 137.5 km. In forming this image, we restricted the imaging procedure so that the reflection from the near-horizontal multiple-generating interface is only on the receiver side. This is consistent with the recording geometry, as the receivers are all to the right of the source, precluding the recording of waves with this reflection on the source-side. The resulting image, made with the sediment velocity model is shown in Figure 5, along with a similar image made in the 1D velocity model. Although these images show a clear salt flank, which is similar to that found in Jones et al. (2007), there is a lot of ringing and a lot of energy far from the expected salt-flank, that detracts from the image quality and the image is relatively low-resolution in the lateral direction. The source of the ringing is likely the same as that in the synthetic example discussed above. We now discuss the attenuation of the energy further from the salt flank; in attenuating it we also gain

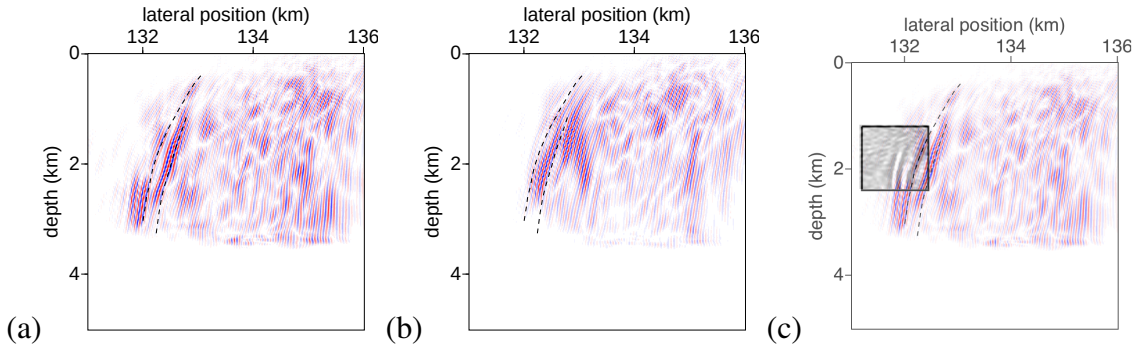

Figure 5: These are doubly-scattered images made with the original data, showing only the region of the model in the dashed box in Figure 4 and (a) the sediment velocity model or (b) the one-dimensional velocity model. (c) Repeats (a) with the image in the box, coming from Jones et al. (2007). Dashed lines mark reflectors picked in Figure 10.

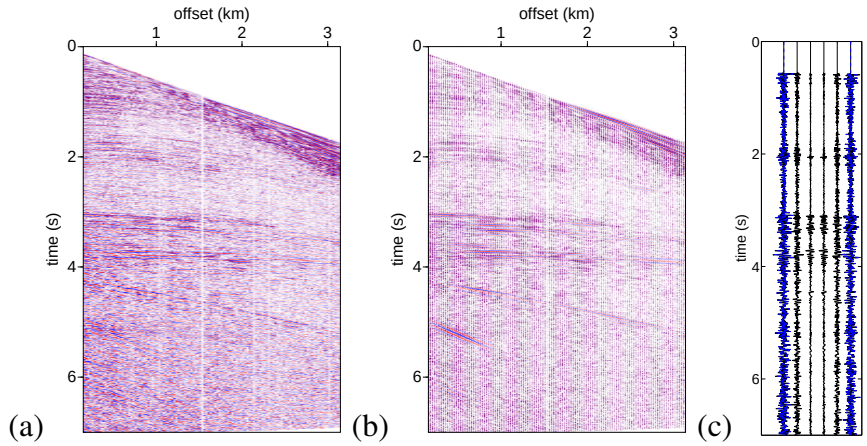

Figure 6: (a) Original shot record with shot at 135 km. (b) Shot record regularized and denoised. (c) Traces from offsets 910 m to 935 m, the black traces are the denoised, regularized traces and the blue lines, which nearly overlay the black, are the original traces at positions where these are available.

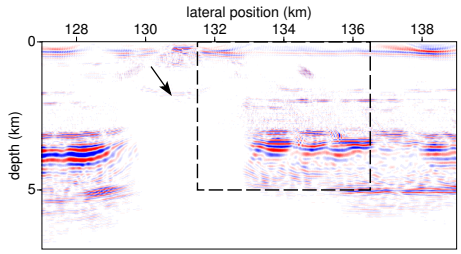

Figure 7: Image made with the regularized and denoised data and the sediment velocity model. The arrow indicates a reflection that could be interpreted as the base of salt.

clues as to its origins.

As a next step, we improve the lateral resolution of the image. Based on the discussion in the previous section, we know that the image of the vertical structure can be improved by simply decreasing the grid size. Although we expect, from that discussion, that simply migrating on a finer grid without increasing the data sampling will improve the image, we decided to first regularize the data because of the large amount of energy far from the salt flank and high general noise level in the image. The regularization procedure used is discussed in the methods section; here we used it to denoise and increase by a factor of 5 the receiver sampling (the regularized offset sampling is 5 m). An example of the resulting regularized data is shown in Figure 6, in which we see that the lateral continuity of the reflections is improved. As shown in Figure 6(c) this regularization procedure fills in traces with smaller amplitudes between the original traces, essentially weighting the interpolated traces less in the migration than the original denoised traces. In the image formed from the regularized data, shown in Figure 7, we already see an improvement in the image. Specifically, the general noise level is reduced and only the more coherent reflectors are still imaged. Although this may not be idea for image interpretation, for our purposes of isolating the multiple-generating interfaces this is an improvement. In addition, the removal of background noise has made a reflector (marked with an arrow) that may be the base of salt stand out more clearly. To image the flank of salt or near-vertical chalk layer, we then repeat the double-scatter imaging with three different velocity/single scatter image pairs, the results of which are shown in Figure 8. It is apparent that while the procedure obviously depends on both the input image and the initial velocity model small changes in these inputs do not result in large changes in the final image.

The data regularization is able to improve the resolution and also to decrease the amount of energy imaging far from the salt flanks, but there are still what appear to be artifacts in the final image. Specifically, there remains a lot of energy relatively far from the expected salt flank location. We expect that these come from primaries reflected from the layers with poor lateral continuity between the chalk layer and the water bottom because such artifacts are not seen in the synthetics and the presence of this reflectivity was not modeled in the synthetic data set. To remove this ringing we now design a surgical muting procedure to isolate, in the

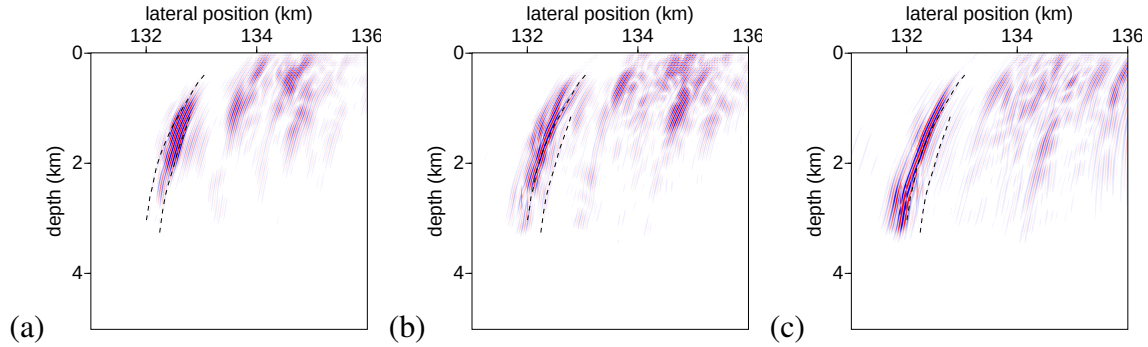

Figure 8: Images made with doubly-scattered waves and the regularized data set, showing only the region in the dashed box in Figure 7. (a) Using the 1D velocity model using a muted version of the image in Figure 7(a) for the estimated reflectivity. (b) Using the sediment velocity model, and a muted version of the image in Figure 7(a) for the estimated reflectivity. (c) Using the sediment velocity and a flat spike reflector at a depth of 3390 m, for the reflectivity; this estimate of the reflectivity does not include a wavelet. In all three subfigures, the dashed lines mark the locations of the salt flanks as picked in Figure 10

data, the doubly-scattered energy between the top of the chalk layer and the salt flank. In the current framework, such a procedure is straightforward, we first mute the double-scatter image to remove what we expect to be artifacts and to isolate the position we think the vertical reflector (salt flank) is in. Second, we isolate the top of the chalk in the regularized image in Figure 7, downsampled back to the original data sampling. It is then straightforward to model the data, using the sources used to form the image, and simply changing the direction of the propagators. This results in a model of the doubly-scattered waves in the data. A surgical mute was then designed by taking data beginning from within a few wavelengths of the modeled doubly-scattered waves, this windowing allows for errors in the modeling from mispositioned reflectors and incorrect smooth velocity, by including data a few wavelengths before the modeled arrival times, but still isolates these events from others in the data. This is illustrated in Figure 9a. The resulting muted data set was then used to construct a doubly-scattered image shown in Figure 10. As this procedure has almost completely removed the energy to the right of the expected salt flank we conclude that these artifacts must have come from events arriving before the doubly-scattered waves that reflect from the salt flank. The most likely candidates for such energy seem to be events (either primaries or multiply-scattered waves) generated by the the somewhat discontinuous reflectors between the top of the chalk and the water bottom.

We then choose the best image of the salt flanks made with doubly-scattered waves to add to the original images to form a final image of the entire region. These final images are shown in Figure 11. Note that the entire imaging procedure was carried out without ever including the salt structure itself in the velocity model.

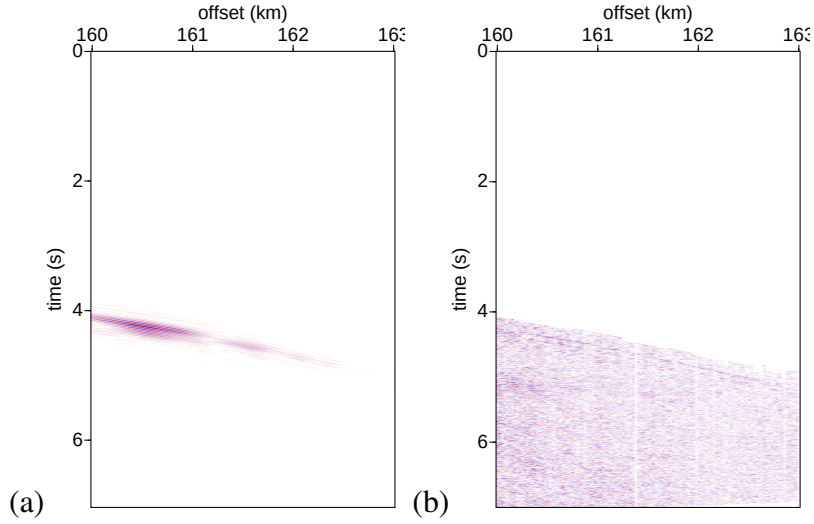

Figure 9: (a) Modelled doubly-scattered data using the top-chalk reflector and the imaged salt flank as the two reflectors. (b) Original data muted with a mute designed to keep only the doubly-scattered data, and later arrivals, based on the modeled data in (a).

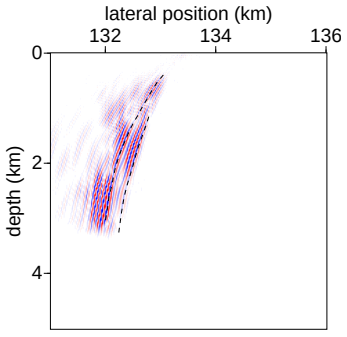

Figure 10: Doubly-scattered image made with the surgically muted data, a muted version of the image in Figure 7(a), and the sediment velocity model. Only the region of the image in the dashed box in Figure 4 is shown here.

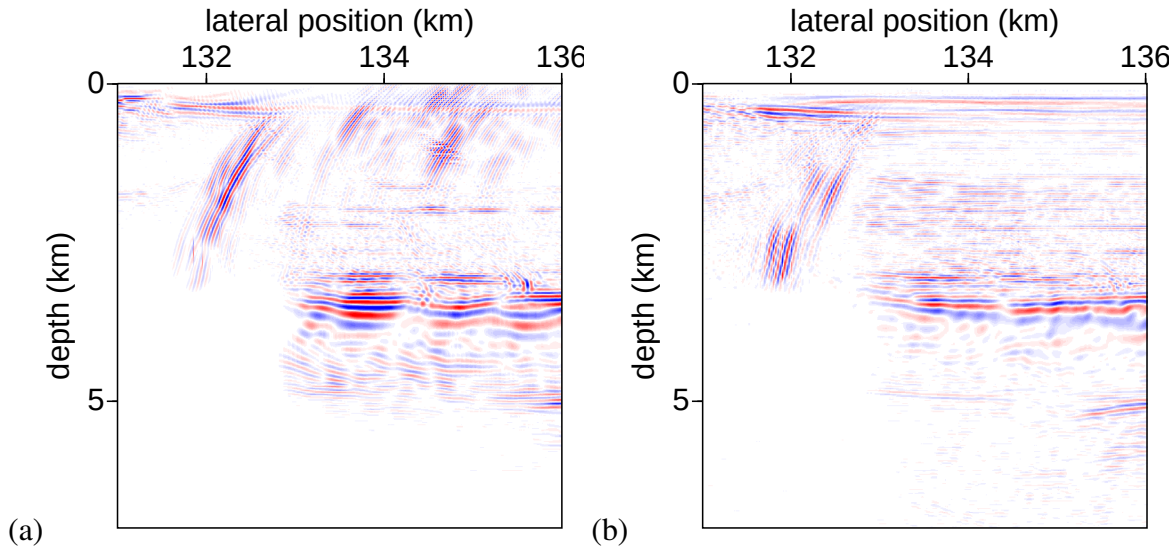

Figure 11: Total images, including both singly and doubly-scattered data, showing only the region of the image in the box in Figure 4, (a) for the regularized data set, using the image in Figure 7 muted outside 3.225 to 3.6 km depth as the estimated reflectivity. The remaining ringing at the salt flank (in this and (b)) may come from multiply-scattered energy in vertical layers adjacent to the salt flank; the artifacts near the surface at around 134 km are likely from energy arriving before the main doubly-scattered arrivals as it is removed in (b) which removes this energy. (b) for the unregularized data set, using the surgically muted data set to make the doubly-scattered image and the image in Figure 4(b) muted outside of 3.225 and 3.6 km as the estimated reflectivity. Note that both images were made entirely with the sediment velocity model.

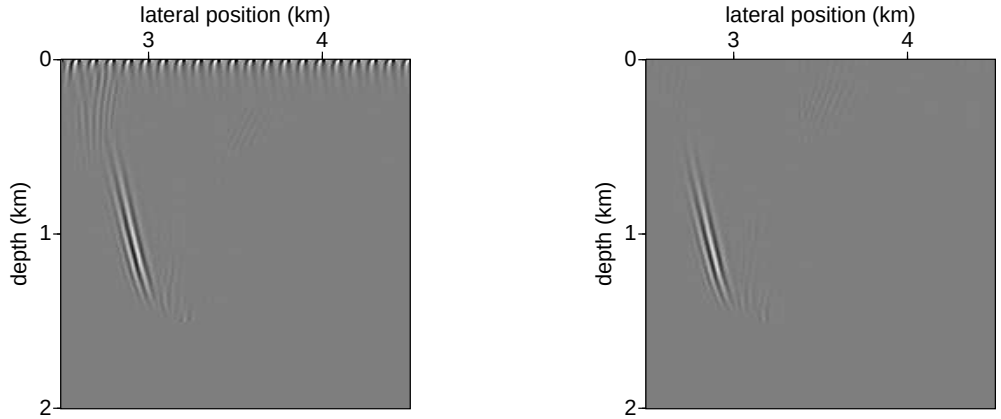

(a) (b)

Figure 12: (a) Image of a simple curved reflector, made with only 10% of the original shot locations. (b) Same as (a) except that this time only 10% of the receivers were used, with the others muted (so the wave propagation is computed on the same grid).

Discussion

Throughout this paper, we have chosen to image only one side of the salt flank because the data set we obtained had data coverage for only one side of the reflector. Given equivalent source/receiver coverage, of course, one can image either side by reciprocity. Motivated by a typical marine acquisition geometry, we study whether or not equivalent illumination of both flanks of the salt is possible. To this end, we use a simple example in which a single near-vertical reflector is imaged. In this example, sources and receivers are simulated every 10 m, with 250 sources from 2.5 to 5 km and 250 receivers with offsets from 0 to 2.5 km. In Figure 12 we show that there is little difference in the recovered image if the sources or receivers are decimated by a factor of 10, to a sampling of 100 m. This highlights the main difference between towing the streamer toward versus away from the flank to be imaged: the difference in sampling of the wave that reflects from the lower layer. This means that imaging with doubly-scattered waves is possible whichever direction the streamer is towed. It is noteworthy, however, that data are required sufficiently far from the flank to allow the recording of doubly-scattered waves. Large offsets are less important, the real data set discussed in this paper had offsets up to little more than 3 km, and only those up to 2 km were used to form the images, however doubly-scattered waves are not likely to be recorded near the salt flank for isolated salt domes like the one used in this study. As mentioned above, the images shown in Figure 12 do not have the ringing seen in both the previous synthetic and real data sets; this indicates that this ringing does not come from either convolution with an extra copy of the wavelet (as this data set uses the same wavelet as the previous synthetic example) or from sharp cut-offs in the fk filter used to separate multiples from primaries (as again this filter is the same here and in the other synthetic example).

Although reverse time migration, or full waveform inversion, are likely to make imaging with one-way methods obsolete in the near future, there is still a place for one-way methods in the determination of the velocity near complicated structures. Even with the added complication of regularization and two-pass one-way methods, it is still faster to make an image in this way than to use reverse-time methods. There is also the added advantage of the ability to separate images made with singly, doubly- and triply-scattered waves. These separate images can be used to identify artifacts from cross-talk (as discussed in detail by Brown and Guitton (2005)), and also for an interpreter to assess the likely artifacts in each image separately. By using an image, rather than including the interface directly in the velocity model, discontinuous or poorly imaged structures may still be used to estimate and thus exploit muliply-scattered waves. Methods such as the two-pass one-way method of Hale et al. (1991) allow the imaging of steep reflectors with turning waves, when such waves are present in the data. The method discussed here, when used to image with doubly-scattered waves, is complementary in that it allows for imaging of steeply dipping reflectors using a multiple-generating interface, rather than requiring a vertical velocity gradient.

Conclusions

We have shown that two-pass one-way methods are able to image near-vertical structures such as salt flanks on real data, allowing the improvement of the understanding of the shape of these salt structures. Imaging with doubly-scattered waves does not require particularly large offsets, but it does require data recorded at some distance from the structure of interest. Sampling is particularly important when imaging vertical structures with small amplitude doubly-scattered waves. We have shown that an ℓ_1 regularization procedure applied to the data, improves each of the steps in the multiply-scattered imaging procedure discussed here. In this particular case, we found that designing a surgical muting procedure to isolate the doubly-scattered phases of interest was helpful in removing imaging artifacts.

Acknowledgements

We are grateful to GX Technologies for the data and permission to publish these results. In particular, Ivan Vasconcelos facilitated the data transfer and made several helpful suggestions and Ian Jones helped to identify and extract a relevant 2D data subset, and provided many of his own figures for comparison. In addition, Rune Mittet was particularly helpful in locating some difficult to find references. BU would like to acknowledge financial support from Statoil through VISTA and the Norwegian Research Council through the ROSE project. MVdH was supported in part by the members of the Geo-Mathematical Imaging Group. AM acknowledges funding from Total and the sponsors of the Earth Resources Laboratory.

References

Andersson, F., M. V. de Hoop, and A. A. Duchkov, 2010, Discrete, almost symmetric wave packets and multi-scale geometrical representation of (seismic) waves: IEEE Transactions on Geoscience and Remote Sensing, in press.

Bell, D. W., 1991, Seismic imaging of steeply dipping geologic interfaces: United States patent.

Berkhout, A. J. and D. J. Verschuur, 2003, Transformation of multiples into primary reflections: SEG Technical Program Expanded Abstracts, **22**, 1925–1928.

——— 2004, Imaging multiple reflections, the concept: SEG Technical Program Expanded Abstracts, **23**, 1273–1276.

——— 2006, Imaging of multiple reflections: Geophysics, **71**, SI209–SI220.

Bernitsas, N., J. Sun, and C. Sicking, 1997, Prism waves – an explanation for curved seismic horizons below the edge of salt bodies: EAGE Expanded Abstracts.

Broto, K. and P. Lailly, 2001, Towards the tomographic inversion of prismatic reflections: SEG Technical Program Expanded Abstracts, **20**, 726–729.

Brown, M. P. and A. Guitton, 2005, Least-squares joint imaging of multiples and primaries: Geophysics, **70**, S79–S89.

Candès, E., L. Demanet, D. Donoho, and L. Ying, 2006, Fast discrete curvelet transforms: Multiscale Model. Simul., **5**, 861–899 (electronic).

Cavalca, M. and P. Lailly, 2005, Prismatic reflections for the delineation of salt bodies: SEG Technical Program Expanded Abstracts, **24**, 2550–2553.

——— 2007, Accounting for the definition domain of the forward map in traveltime tomography – application to the inversion of prismatic reflections: Inverse Problems, **23**, 139–164.

Daubechies, I. and G. Teschke, 2005, Variational image restoration by means of wavelets: simultaneous decomposition, deblurring, and denoising: Appl. Comput. Harmon. Anal., **19**, 1–16.

de Hoop, M. V., 1996, Generalization of the Bremmer coupling series: J. Math. Phys., **37**, 3246–3282.

Farmer, P. A., I. F. Jones, H. Zhou, R. I. Bloor, and M. C. Goodwin, 2006, Application of reverse time migration to complex imaging problems: First Break, **24**, 65–73.

Ferguson, R. J. and G. F. Margrave, 2002, Prestack depth migration by symmetric nonstationary phase shift: Geophysics, **67**, 594–603.

Gazdag, J. and P. Sguazzero, 1984, Migration of seismic data by phase shift plus interpolation: Geophysics, **49**, 124–131.

Hale, D., N. R. Hill, and J. P. Stefani, 1991, Imaging salt with turning seismic waves: SEG Technical Program Expanded Abstracts, **10**, 1171–1174.

Hawkins, K., 1994, The challenge presented by North Sea Central Graben salt domes to all DMO algorithms: First Break, **12**, 327–343.

Hennenfent, G. and F. J. Herrmann, 2006, Seismic denoising with nonuniformly sampled curvelets: Computing in Science and Engineering, **8**, 16–25.

Jiang, Z., 2006, Migration of interbed multiple reflections: SEG Technical Program Expanded Abstracts, **25**, 3501–3505.

Jiang, Z., J. Sheng, J. Yu, G. T. Schuster, and B. E. Hornby, 2007, Migration methods for imaging different-order multiples: Geophysical Prospecting, **55**, 1–19.

Jiang, Z., J. Yu, G. T. Schuster, and B. E. Hornby, 2005, Migration of multiples: The Leading Edge, **24**, 315–318.

Jin, S., S. Xu, and D. Walraven, 2006, One-return wave equation migration: Imaging of duplex waves: SEG Technical Program Expanded Abstracts, **25**, 2338–2342.

Jones, I. F., M. C. Goodwin, I. D. Berranger, H. Zhou, and P. A. Farmer, 2007, Application of anisotropic 3D reverse time migration to complex North Sea imaging: SEG Technical Program Expanded Abstracts, **26**, 2140–2144.

Kostyukevych, A., N. Marmalevskyi, Y. Roganov, and V. Roganov, 2009, Analysis of azimuthally-dependent transmission coefficients of converted PS-waves for duplex migration on transmitted waves: SEG Technical Program Expanded Abstracts, **28**, 1257–1261.

Link, B., N. Marmalevskyi, Y. Roganov, A. Kostyukevych, and Z. Gornyak, 2007, Direct imaging of subtle, zero-throw vertical faulting — a 3D real-data example: SEG Technical Program Expanded Abstracts, **26**, 2359–2363.

Malcolm, A., B. Ursin, and M. de Hoop, 2009, Seismic imaging and illumination with internal multiples: Geophysical Journal International, **176**, 847–864.

Malcolm, A. E. and M. V. de Hoop, 2005, A method for inverse scattering based on the generalized Bremmer coupling series: Inverse Problems, **21**, 1137–1167.

Marmalyevskyy, N., Y. Roganov, Z. Gornyak, A. Kostyukevych, and V. Mershchiy, 2005, Migration of duplex waves: SEG Technical Program Expanded Abstracts, **24**, 2025–2028.

Marmalyevskyy, N., Y. Roganov, A. Kostyukevych, and V. Roganov, 2008, Duplex wave migration and interferometry for imaging onshore data without angle limitations: EAGE Expanded Abstracts.

Métivier, L., F. Delprat-Jannaud, L. Halpern, and P. Lailly, 2009, 2D nonlinear inversion of walkaway data: SEG Technical Program Expanded Abstracts, **28**, 2342–2346.

Mittet, R., 2002, Multiple suppression by prestack reverse time migration: A nail in the coffin: EAGE Expanded abstracts.

——— 2006, The behaviour of multiples in reverse-time migration schemes: EAGE Expanded abstracts.

Muijs, R., J. O. A. Robertsson, and K. Holliger, 2007, Prestack depth migration of primary and surface-related multiple reflections: Part I — Imaging: Geophysics, **72**, S59–S69.

Reiter, E. C., M. N. Toksöz, T. H. Keho, and G. M. Purdy, 1991, Imaging with deep-water multiples: Geophysics, **56**, 1081–1086.

Schuster, G. T., J. Yu, J. Sheng, and J. Rickett, 2004, Interferometric/daylight seismic imaging: Geophysical Journal International, **157**, 838–852.

Stolt, R., 2002, Seismic data mapping and reconstruction: Geophysics, **67**, 890–908.

Vasconcelos, I., R. Snieder, and B. Hornby, 2007, Target-oriented interferometry — Imaging with internal multiples from subsalt VSP data: SEG Technical Program Expanded Abstracts, **26**, 3069–3073.

Weglein, A., F. B. Araújo, P. M. Carvalho, R. H. Stolt, K. H. Matson, R. T. Coates, D. Corrigan, D. J. Foster, S. A. Shaw, and H. Zhang, 2003, Inverse scattering series and seismic exploration: Inverse Problems, **19**, R27–R83.

Xu, S. and S. Jin, 2006, Wave equation migration of turning waves: SEG Technical Program Expanded Abstracts, **25**, 2328.

——— 2007, An orthogonal one-return wave-equation migration: SEG Technical Program Expanded Abstracts, **26**, 2325–2329.

Youn, O. K. and H. Zhou, 2001, Depth imaging with multiples: Geophysics, **66**, 246–255.

Zhang, Y., S. Xu, and G. Zhang, 2006, Imaging complex salt bodies with turning-wave one-way wave equation: SEG Technical Program Expanded Abstracts, **25**, 2323.